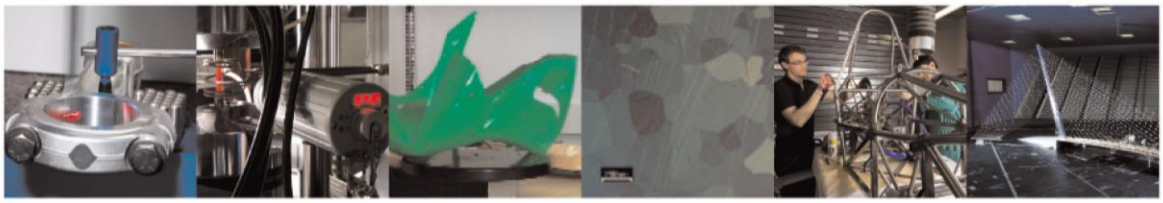

Cold Spray Deposition of Freestanding Inconel Samples and Comparative Analysis with Selective Laser Melting

Bagherifard, Sara; ROSCIOLI, GIANLUCA; ZUCCOLI, MARIA VITTORIA; HADI, MEHDI; D'ELIA, GAETANO; Demir, Ali Gökhan; Previtali, Barbara; Kondás, Ján; Guagliano, Mario

This is a post-peer-review, pre-copyedit version of an article published in JOURNAL OF THERMAL SPRAY TECHNOLOGY. The final authenticated version is available online at: http://dx.doi.org/10.1007/s11666-017-0572-3]

Cold Spray Deposition of Freestanding Inconel Samples and Comparative Analysis with Selective Laser Melting

Sara Bagherifard[1], Gianluca Roscioli[1], Maria Vittoria Zuccoli[1], Mehdi Hadi[2], Gaetano D'Elia[2], Ali Gökhan Demir[1], Barbara Previtali[1], Ján Kondás[3], Mario Guagliano[1*]

[1]Politecnico di Milano, Department of Mechanical Engineering, Via La Masa 1, 20156, Milan, Italy
[2]Politecnico di Torino, Department of Mechanical and Aerospace Engineering, corso Duca degli Abruzzi 24, Turin, Italy
[3]Impact Innovations GmbH, Bürgermeister-Steinberger-Ring 1, 84431 Haun/Rattenkirchen, Germany

Abstract: Cold spray offers the possibility of obtaining almost zero-porosity build-ups with no theoretical limit to the thickness. Moreover, cold spray can eliminate particle melting, evaporation, crystallization, grain growth, unwanted oxidation, undesirable phases and thermally induced tensile residual stresses. Such characteristics can boost its potential to be used as an additive manufacturing technique. Indeed, deposition via cold spray is recently finding its path towards fabrication of freeform components since it can address the common challenges of powder-bed additive manufacturing techniques including major size constraints, deposition rate limitations and high process temperature.

Herein, we prepared Nickel-based super alloy Inconel 718 samples with cold spray technique and compared them with similar samples fabricated by selective laser melting method. The samples fabricated using both methods were characterized in terms of mechanical strength, microstructural and porosity characteristics, Vickers microhardness and residual stresses distribution. Different heat treatment cycles were applied to the cold sprayed samples in order to enhance their mechanical characteristics. The obtained data confirm that cold spray technique can be used as a complementary additive manufacturing method for fabrication of high quality freestanding components where higher deposition rate, larger final size and lower fabrication temperatures are desired.

Keywords: Cold spray, additive manufacturing, selective laser melting, Inconel 718

1. Introduction:

The latest trend in rapid manufacturing of three-dimensional free-standing (3D) forms, known as 3D-printing, direct digital manufacturing and additive manufacturing (AM), has become the focus of current research in the past several years. The efficiency and flexibility in fabrication of complex geometries and customized structures offered by AM techniques can eliminate many costly intermediate steps commonly used within traditional manufacturing approaches and reduce the waste of materials. AM techniques are directly linked to digital design tools and thus can offer the possibility of direct production of highly customizable products through a layer by layer fabrication methodology; while the traditional methods necessitate fabrication of new molds, dies and tools for design alterations and thus bid limited flexibility at higher production costs. Two key features in categorizing the ever growing wide variety of AM techniques and apparatus are the material feed system (powder bed, powder feed and wire feed) and energy source (electron beam, laser, arc) [1]. In majority of the developed methods, the material undergoes extreme heating which result in melting followed by solidification. Some materials are also reported to be subjected to continual solid state phase transformations during these AM techniques [1]. Such complex history can result in peculiarities in the microstructure and the resultant mechanical properties of the fabricated part. Selective laser melting (SLM), laser sintering (LS), laser metal deposition (LMD) as well as wire fed laser beam (WFLB), laser engineered net shaping (LENS) and laser beam powder bed (LBPB) are some of the major laser based AM techniques and their variants regarded as some of the most versatile AM techniques. This highlights the wide application and acceptability of laser in AM field [2-4]. With the notable progress in AM technology during the last decade, its applications that started from rapid

prototyping have evolved to rapid manufacturing of end-use products in a wide range of applications [5]. Currently, AM technologies are taking a fast pace towards fabrication of geometrically and functionally complex structures for a wide range of applications, rapidly establishing their position in mainstream manufacturing [6]. Cold spray (CS), as a fast growing deposition method principally used as a coating technology [7, 8], is gaining considerable attention for direct production of freestanding components rather than deposition of surface coatings, due to its ability to create thick buildups, with no theoretical limit to the size and the thickness. Several centimeters thick deposits are reported to be obtained by CS using various feedstock powders at much higher deposition and productivity rates compared to common AM techniques [7, 9]. Compared to powder-bed fusion such as selective laser melting (SLM) and electron beam melting (EBM) [10] and directed energy deposition techniques employing laser or electron-beams [1], the absence of heat and hence phase transformation provide several advantages. CS is known to result in properties that are pre-requisites to fabrication of high-quality metal build-ups including structural homogeneity, high density, high purity, notable cohesive strength and frequently moderate compressive residual stresses [7, 8, 11, 12]. Moreover, the cold nature of CS process, which ensures solid-state deposition, eliminates the risk of melting, oxidation, thermal decomposition, crystallization and grain growth as well as formation of undesirable phases [13]. These characteristics make CS commendable for spraying temperature sensitive materials including nanostructures, nanocomposites and amorphous materials [14-16], as well as oxygen sensitive materials such as aluminum, copper, and titanium [17-19]. Finally yet importantly, the multi-material deposition possibility can significantly boost the potential of CS as an AM technology [20]. On the other hand, compared to AM technologies employing laser and electron beam heat sources, the CS techniques lack precision and require comprehensive finishing operations. Some of the advantages of powder-bed fusion processes such as internal channels and production of lattice structures without the need of masks or dies are not present [21, 22]. However, in general there is an apparent lack of detailed investigations between CS and more conventional AM technologies based on melting.

Earlier studies demonstrated the feasibility of adapting CS technique for fabrication of freestanding components using variety of materials including Ti, Al, stainless steel, Cu and Zn [23-26]. The process consists in controlling powder feed rate and nozzles spatial velocity and movements to follow the outer contours of a suitably shaped substrate and obtain a near-net shape object. The last step is to detach the three-dimensional form from the substrate and perform the desired final finishing steps [7]. Lynch et al. [27] performed a topology optimization study, developing design guidelines, for fabrication of cold sprayed free standing components. As a proof of concept, Pattison et al. [28] demonstrated the possibility of obtaining multi-material deposition, internal channels and embedded devices by CS using different materials and different deposition strategies. Geometries that are more elaborate have been recently obtained by CS using commercially available wire mesh masks to fabricate freestanding pyramidal fin arrays of various sizes for heat exchangers with excellent heat transfer performance even higher than that of the traditional fins [29].

In light of the emerging attention in CS as an AM technique, this research is aimed at assessing the potential of CS for fabrication of freestanding Inconel components. Precipitation hardenable nickel-based super alloy Inconel 718 is commonly used for service in harsh environments subjected to extreme pressure and temperature, for instance in jet engine and gas turbines. Production costs of Inconel components using traditional fabrication techniques is quite high due to shaping and machining difficulties; thus it would be interesting to find an efficient AM technique for fabrication of high quality Inconel based materials. Standard dog bone samples were fabricated by CS and were compared with those produced by selective laser melting (SLM) method, as one of the most diffused AM technologies. SLM is based on powder bed fusion using high-power laser beam and is widely used to produce a variety of intricate geometries. There are limited studies investigating the characteristics of cold sprayed Inconel coatings. Karthikeyan and Kay [30] were the first to report deposition of Inconel 718 by CS method. Morocco et al. [31] used both fine and coarse feedstock powder to produce quite high density Inconel 718 CS coatings with a relatively low bond strength. Levasseur et al. [32] used CS to deposit Inconel 718 on mild steel substrates. They obtained a high porosity of around 3% and low mechanical strength and thus applied subsequently a series of pressure-less sintering processes to successfully decrease the porosity of the obtained coating and enhance its mechanical strength. Wong et al. [33] deposited thick coatings of Inconel 718 using

different CS conditions and studied the effect of multiple heat treatments on microstructure, porosity and tensile properties of the deposited material. They showed the efficiency of heat treatments in enhancing mechanical strength and ductility of the Inconel depositions. More recently, Huang and Fukanum [34] deposited Inconel 718 by CS and studied the effect of propellant gas (He and N_2) on the mechanical characteristics of the deposited material. Adhesion and cohesion strength tests revealed higher quality for the material deposited by He; however, the mechanical characteristics of the material deposited by N_2 was also significantly increased after post-spray heat treatment.

In this study, in order to compare CS and SLM Inconel 718 samples, the microstructural and mechanical properties of both series of samples were analyzed using optical and scanning electron microscopy (SEM), porosity, microhardness and residual stress measurements. Two different annealing heat treatments were applied to the CS samples in order to enhance ductility of the material. Due to some practical limitations caused by the prototype SLM machine, which limited the total number of standard sized SLM samples, these series have been studied just in as built condition. Static tensile tests were performed on samples before and after heat treatments and the results were compared with those of SLM samples and bulk material. The effect of spray direction as well as post spray heat treatments were evaluated on the properties of the CS material. The obtained data indicate that CS is a promising method for fabrication of high quality Inconel 718 components. The results confirmed that the applied heat treatments resulted in significant ductility enhancement of the as-sprayed material. The effect of spray direction was found insignificant on CS samples' characteristics.

2. Experimental procedure

2.1 Feedstock Powder

Commercially available gas-atomized Ni-based alloy Inconel 718 powder (Praxair Surface Technologies, US) with a typical chemistry composition of (Ni-19Cr-18Fe-Nb+5Ta-3Mo-1Ti) was used for fabrication of both CS and SLM samples in order to eliminate the effect of particle variables in the final comparisons. SEM micrograph of the quite smooth and almost spherical powders with diameters ranging between 10-32 µm (average size of ~15 µm) is shown in Fig. 1(a).

2.2 Sample Preparation

2.2.1 Cold Spray samples and Heat Treatments

CS samples were sprayed on Al substrates Impact Spray System 5/11 (60bar upgrade; Impact Innovations GmbH, Haun, DE). The spray parameters are listed in Table 1. A thick deposition of 120×100×4 mm, grown on an Al substrate was cut and machined to obtain dog bone specimens (Fig. 1(b)), based on standard test methods for tension testing of metallic materials (ASTM E8/E8M–15a).

Two different sets of samples were cut in longitudinal (L) and transversal (T) directions with respect to the spray direction, in order to evaluate the effect of the latter parameter in mechanical characteristics of the obtained deposition. Two annealing heat treatments were applied to the CS samples; the first heat treatment (HTA) was performed at 1050°C for 3 h (TZF 12/75/700 Carbolite furnace) and the second one (HTB) at 1200°C for 1 h (LHT02/17LB by Nabertherm furnace). Both treatments were performed under 100% argon atmosphere and the samples were let to cool down to room temperature while maintaining continuous argon gas flow inside the chambers. A Rockwool layer was used for both heat treatments, to prevent samples' adhering to the internal walls of the chambers.

2.2.2 Selective Laser Melting Samples

A prototype SLM system, namely Powderful, designed and assembled in the Department of Mechanical Engineering at Politecnico di Milano was used in this study, allowing for flexible control over the whole process parameters. The system was equipped with a multimode fibre laser source with 1 kW maximum power (IPG

Photonics YLR-1000, Cambridge, MA, USA) and a scanner (El.En. Scan Fiber, Florence, IT). Scan trajectory was designed using LogoTag software (Taglio, Piobesi D'alba, IT). The scan head housed a 60 mm collimating lens and a 255 mm f-theta lens, producing 212 µm beam diameter at focal plane. Table 2 reports the main specifications of the SLM system. The system allowed for operating in controlled processing chamber. Initially, vacuum was applied down to 50 mbar pressure and then argon gas was flooded. The procedure was repeated 3 times before starting samples preparation under Ar atmosphere. In the present configuration, process variables to be optimized for fabrication of Inconel samples, were considered as laser power and scan speed, while hatch distance between adjacent scan tracks and layer thickness were kept constant, i.e. 110 µm and 50 µm correspondingly. Nine small cubic samples (see Fig. 1 (c)) were prepared with various combinations of laser power (200, 250 and 300 W) and scan speed (100, 150 and 200 mm/s). Details of the experimented conditions are reported in Table 3. The cubic samples were evaluated in terms of porosity and microhardness, as will be described in the following sections; based on the porosity data, the optimal parameters were chosen for fabrication of final dog bone SLM samples.

2.3 Characterization Methods

All the characterizing methods were performed on CS samples before and after heat treatments in both longitudinal and transversal directions and for SLM sample.

Samples' porosity was assessed through performing image analysis on the polished cross sections. For each three images were acquired with SEM (Zeiss Evo MA 15). Samples' density was also calculated as another indication of porosity using a density determination kit working based on Archimedean buoyancy principle (Precisa 100A-300M, Turin, IT). In this method, the weight of the samples measured in air and water was used to determine their density using Eq.1:

$$\rho = \frac{W_{air}\rho_{liquid}}{W_{air}-W_{liquid}} \quad (1)$$

where W_{air}, W_{liquid}, and ρ_{liquid} are the weight of the sample in air, its weight in water and the density of water (0.99823 g/cm^3 at standard conditions). Finally, the obtained density was compared to the density of bulk material (8.19 g/cm^3 for Inconel 718) to provide an estimation of the porosity.

For cross-sectional microstructural analysis, the samples were cut, impregnated in hot mounting resin and ground with SiC papers up to P2500, followed by a micro-polishing step using diamond suspensions of 6, 3 and 1 micrometers scratch size sequentially. The polished surfaces were chemically etched (10 parts of HCl (37%) and 3 parts of H_2O_2) for 4 seconds. Lastly, samples' surfaces were observed by optical microscope using bright light at different magnifications. Tensile strength of the samples was evaluated by a Universal MTS test system at a displacement rate of 2 mm/min following ASTM E8 specification using samples with a gage length of 25 mm, gauge width of 6 mm and thickness of 4 mm. Fracture surface of the failed samples were examined using a Zeiss-Evo 50 SEM microscope. Microhardness measurements were performed on polished cross section of the samples using microhardness tester FM-700 (Future-Tech, JP) with a diamond Vickers indenter. Based on the samples' geometry, Vickers indentations were performed at different distances from the edges with a force of 300 gf and dwell time of 15 s.

The profile of the residual stresses was characterized using AST X-Stress 3000 portable X-ray diffractometer emitting Cr$K\alpha$ radiation ($\lambda_{K\alpha}$=2.2898Å) for Inconel 718. Measurements were performed using $\sin^2(\psi)$ method, diffraction angle of 128° for Inconel 718 (calibrated using microstrain free standard Ni sample at 133.5°) scanned with a total of 11 Chi tilts in the range of −45° to 45° along three rotations of 0°, 45° and 90°. Measurements were carried out in depth, sequentially removing a thin layer of material through electro-polishing with a solution of acetic acid (94%) and perchloric acid (6%).

3. Results and Discussion

3.1 Porosity Assessment

Average porosity data obtained for SLM optimized sample as well as CS longitudinal and transversal samples, before and after the two heat treatments are reported in Fig. 2. The data indicate that for all the samples, image analysis methodology shows much lower porosity compared to the ones obtained from density measurements. This notable difference can be attributed to the intrinsic differences between the two methodologies; the density determination kit data are based on volumetric porosity. The data obtained from optical micrographs analysis are based on cross-section image analysis and consider isotropy along the cross section of the specimens. On the other hand, measurements over cross-section images have also been shown to be accurate in literature for high density conditions [35]. Besides, surface imperfections and finishing allowances at borders of SLM samples can cause relevant errors in the density based approach, while in image analysis such defects can be manually eliminated from the analyzed area. However, both series of data present a similar trend of porosity variation between samples.

The porosity results indicated no notable differences between transversal and longitudinal CS samples. The obtained data confirm that SLM samples have lower porosity compared to CS ones. The partial interparticle bonding in the as sprayed condition promotes microdefects and porosities in the deposition matrix, which are mainly formed at the particle-particle interface [32, 36]. The applied heat treatments seem to have in general decreased porosity of CS and increasing the annealing temperature did not show further influence on the porosity of CS samples. This pore reduction can be attributed to the additional metallurgical bonding that could have occurred at high temperatures as a result of sintering effect.

Optical micrographs of the nine cubic SLM samples, fabricated using different process parameters, were analyzed to evaluate samples' porosity. The results indicated that the optimal set of parameters to minimize porosity were laser power of 200 W and scan speed of 100 mm/s (highlighted in Fig. 3(a)). As confirmed by the data obtained from density determination kit, these results indicated that higher laser scanning speed increased samples' porosity.

3.2 Microstructural Characterization

Cross section microstructural comparisons revealed essentially different features in the grain structure of CS and SLM samples. The CS sample before heat treatment (Fig. 3(c)) showed relatively small grains with evident signs of significant particle deformation. The boundaries are plainly visible between adjacent deformed particles. Inside individual particles, a dendritic structure, which is characteristic tree-like structure of atomized crystals of the powders, can be observed. This dendritic structure that is present throughout the whole structure, confirms that the CS process has not affected the original structure of particles during deposition. Due to the similarity of the microstructural features in CS longitudinal and transversal samples at all conditions, just the micrographs of longitudinal samples are presented here for the sake of brevity.

Cross section of the SLM sample parallel to laser scanning direction (Fig. 3(b)), on the other hand, shows a relatively coarse columnar structure. The observations represent formation of very small dendrites and columnar structures inside coarse grains, which could be mainly formed during solidification of the melt pool.

As reported by Levasseur et al. [32], limited deformation of Inconel 718 upon impact reduces the chances to form metallurgical bonding and thus application of proper heat treatments have been always perused in order to promote mechanical strength in CS deposited Inconel. Here we applied two different heat treatments, after both of which, recrystallization and the formation of coarser grains can be observed within the matrix of the CS samples. Grain boundaries seem to fade after annealing treatment and the dendritic structure almost disappeared resulting in formation of a more uniform structure. Similar results on partial disappearance of interparticle boundaries after heat treatment was reported in previous studies where it was attributed to some

sintering effect caused by high temperatures applied during heat treatments [33]. In case of HTB, even more recrystallization occurred and twin boundaries could be observed in many grains.

3.3 Tensile Strength and Fractography

Tensile test results indicated that CS samples with no heat treatment present low tensile strength and almost zero ductility; whereas, SLM samples represent comparable tensile strength but considerably higher ductility. Poor interparticle bonding, as suggested by similar reports [32, 37], could be the key responsible for the quite brittle nature of the as sprayed samples. Yet again, no significant difference was observed between longitudinal and transversal samples' mechanical strength.

After heat treatments, a transition from brittle to ductile behavior was observed. The heat treatments were found to decrease porosity and enhance the bonding between the particles, leading to higher cohesive strength of the deposited material. The tensile strength and ductility of the heat treated samples were significantly improved to varying levels depending on the applied treatment, as also reported by Wong et al. [33] who evaluated the effect of heat treatments to enhance the mechanical strength of CS Inconel 718 coatings. The HTB sample represented higher ductility compared to the SLM one, even comparable to that of bulk material in a wide range of heat treatment and aging conditions [34, 38]. Increased ductility and mechanical strength can be attributed to the better interparticle metallurgical bonding as well as higher structural homogeneity and pore reduction, which resulted from the sintering effect that occurred at high temperatures. The results of the tensile tests and the engineering stress strain curves for all samples are shown in Table 4 and Fig. 4, respectively. Fracture surfaces of failed samples observed by SEM are shown in Fig. 5. Fracture surface of SLM sample, indicated the presence of relatively large pores and cavities that could be formed due to the limitations of the prototype SLM machine used in this study. Indeed, this prototype machine was originally made for fabrication of small samples as the cubic ones (10×10×10 mm) used for process parameters optimization. The thermal dissipation limitations caused during fabrication of relatively large standard dog bone samples required to stop the manufacturing process intermittently to cool the system and the substrate down. These pores could have reduced the tensile strength of the SLM samples; however, numerous small dimples that are characteristics of ductile fractures can be observed on the fracture surface of SLM samples (Fig. 5(b)), which can be accountable for the notable sample elongation of 12.6% before final rupture.

The CS sample before heat treatment (Fig. 5(c)), as expected from tensile test data, represents bright fracture surface, indicating brittle fracture as a consequence of a mixed mechanism of inter-splat and intra-splat fracture. Similar interparticle failure were reported also by Levasseur et al. [32] who observed no signs of adhesion or ductility on the fracture surfaces of as sprayed Inconel 718 deposits. A mixture of round shaped areas, typical of whole splat detachment (cyan arrows) and areas where cleavage and intra splat fracture (red arrows) occurred are observed with no indications of dimples Fig. 5(c), showing low cohesion strength of the deposited material without heat treatment. After HTA, a clear transition from relatively brittle behavior was demonstrated to higher ductility, and the fracture surfaces suggest a mixed ductile–brittle fracture mode. HTB samples showed even further mechanical strength and ductility enhancement. Reduction of porosity, recrystallization and formation of twin boundaries seem to have transformed the structure towards even more ductile behavior after HTB. Fracture surfaces of heat treated samples revealed mutually intergranular fracture and cleavage; the appearance of dimples on the fracture surfaces are a proof of the increased ductility. After HTB higher fraction of dimple features were observed immersed in the fragile matrix compared to HTA, indicating that overall ductility increased with increasing annealing temperature. These observations surfaces correlate well with the tensile strength test data.

3.4 Microhardness Measurement

Microhardness was measured on different areas close to the surface of the samples and at the core material. The results showed no notable microhardness variation at different positions on the cross sections of all samples indicating the homogeneity of both CS and SLM process; no difference was measured between longitudinal and transversal CS samples' hardness either.

The results of the measurements performed on longitudinal and transversal CS samples before and after heat treatments as well as the measurements performed on all nine SLM cubes (number 1 representing the optimized condition) are shown in Fig. 6. As it can be observed in Fig. 6, the two heat treatments caused notable material softening, decreasing the hardness of CS samples from 530 HV to around 400 HV. The softening effect of annealing treatment overshadowed the positive effect of reduced porosity on the hardness. In comparison, the SLM samples show much lower hardness of around 300 HV; this can be attributed to the coarser and softer crystalline structure after melting and solidification compared to the dendritic and recrystallized structure of CS samples. Stain hardening effect caused by particle impacts during deposition could also contribute to the increased hardness.

3.5 Residual Stress Measurement

In depth distribution of residual stresses is presented in Fig. 7(a). The plastic deformation caused by high energy impacts of powders during CS process and the post deposition machining of the samples could both contribute to the development of compressive residual stresses. In order to separate the effect of these two features, the distribution of residual stresses was measured also on as sprayed samples before machining. Negligible residual stresses were found on the as sprayed CS samples; whereas, as machined CS samples showed considerable compressive residual stresses especially in the layers close to the surface. Thus, the residual stresses in CS samples were concluded to be mainly due to the machining process rather than to CS coating process itself. The results indicated that these compressive residual stresses tend to relax after heat treatments. After HTA, maximum compressive residual stress of -450 is partially relaxed reaching -300 MPa; however, still a remarkable depth of material (0.06-0.08 mm) was characterized by compressive stresses.

After HTB, more substantial indications of stress relaxation were expected; nonetheless, the distribution of stresses after HTB were quite similar to that of HTA and even slightly higher at some depths. We postulate that this variation can be caused by the formation of a thin oxide film on the sample's surface after HTB, as in this case in the absence of a vacuum system to entirely remove oxygen before pumping argon inside the furnace chamber, sample's oxidation could no be fully avoided. The volume increase and expansion caused by surface oxidation at higher temperature while the underlying layers were more constrained by the bulk material, could have induced compressive residual stresses at the surface. Thus, the counteracting effects of annealing treatment and surface layer oxidation lead to minimal change of distribution of residual stresses in HTB samples. These compressive residual stresses are expected to enhance the fatigue strength of the CS samples under cyclic loading.

Regarding the SLM sample, significantly high tensile residual stresses were measured at the surface up to a depth of around 150 μm; these thermally induced tensile stresses are principally caused by the high temperature gradient mechanism on which SLM processes are commonly based.

Another parameter that was extracted from XRD measurements is full with of the diffraction peak at half of its maximum intensity (FWHM). FWHM can be considered as an indication of hardness, grain size and micro strain. The results, as presented in Fig. 7(b), point out that as sprayed and as machined CS samples have similar FWHM values. After annealing treatments, yet, The FWHM data of CS samples become identical to that of SLM sample, representing that the applied heat treatments lead to recover some ductility, as also confirmed by the tensile tests.

4. Conclusions

In this study, the possibility of using cold spray process as a non-thermal additive manufacturing method was assessed and compared with the results obtained from selective laser melting method that is a well-known and widely used additive manufacturing technique. The major results of the present study are listed below:

- Highly dense thick Inconel 718 buildups were prepared by cold spray technique.
- The spraying direction was found not to affect the microstructure and mechanical properties of the cold spray deposited material.
- As sprayed samples show very limited ductility; however, with appropriate heat treatment, porosity was reduced, interparticle bonding was enhanced and comparable mechanical strength and ductility with bulk Inconel 718 were obtained.
- Increasing the annealing temperature further promoted material softening, as confirmed by fractographic observations, which revealed increasing fraction of dimples on the fracture surfaces by enhancing annealing temperature.
- Contrary to SLM sample with high tensile residual stresses caused by high rate of thermal fluctuations, notable compressive residual stresses were measured on the surface layer of the CS samples, which were stable also after heat treatments.

To come to the point, the obtained results imply that cold spray permits to elaborate dense freeform 3D Inconel 718 objects with high cohesive strength. Cold spray technique is considered of high potential to be used for fabrication of freestanding components as an alternative to common additive manufacturing techniques particularly where restrictions caused by the final product size, degradation risk of the feedstock material and/or deposition rate come into play. On the other hand, for a more comprehensive analysis, heat treatment of the SLM produced components and their performance should be assessed. The complementary aspects of the two processes should be evaluated furthermore considering the process resolution and finishing operations required to reach the final component form.

Acknowledgments

The authors declare no conflict of interests in this work. GR, MVZ, MH and GD acknowledge financial support from Alta Scuola Politecnica (ASP).

References

[1] Frazier WE. Metal additive manufacturing: a review. Journal of Materials Engineering and Performance. 2014;23:1917-28.

[2] Kumar S, Pityana S. Laser-based additive manufacturing of metals. Advanced Materials Research: Trans Tech Publ; 2011. p. 92-5.

[3] Gu D, Meiners W, Wissenbach K, Poprawe R. Laser additive manufacturing of metallic components: materials, processes and mechanisms. International materials reviews. 2012;57:133-64.

[4] Murr LE, Gaytan SM, Ramirez DA, Martinez E, Hernandez J, Amato KN, et al. Metal fabrication by additive manufacturing using laser and electron beam melting technologies. Journal of Materials Science & Technology. 2012;28:1-14.

[5] Guo N, Leu MC. Additive manufacturing: technology, applications and research needs. Frontiers of Mechanical Engineering. 2013;8:215-43.

[6] MacDonald E, Wicker R. Multiprocess 3D printing for increasing component functionality. Science. 2016;353:aaf2093.

[7] Champagne V, Helfritch D. The unique abilities of cold spray deposition. International Materials Reviews. 2016;61:437-55.
[8] Ghelichi R, Guagliano M. Coating by the Cold Spray Process: a state of the art. Fracture and Structural Integrity. 2009:30-44.
[9] Pattison J, Celotto S, Morgan R, Bray M, O'Neill W. Cold gas dynamic manufacturing: A non-thermal approach to freeform fabrication. International Journal of Machine Tools and Manufacture. 2007;47:627-34.
[10] Murr LE, Martinez E, Amato KN, Gaytan SM, Hernandez J, Ramirez DA, et al. Fabrication of metal and alloy components by additive manufacturing: examples of 3D materials science. Journal of Materials Research and technology. 2012;1:42-54.
[11] Ghelichi R, MacDonald D, Bagherifard S, Jahed H, Guagliano M, Jodoin B. Microstructure and fatigue behavior of cold spray coated Al5052. Acta Materialia. 2012;60:6555-61.
[12] Ghelichi R, Bagherifard S, MacDonald D, Fernandez-Pariente I, Jodoin B, Guagliano M. Experimental and numerical study of residual stress evolution in cold spray coating. Applied Surface Science. 2014;288:26-33.
[13] Assadi H, Kreye H, Gärtner F, Klassen T. Cold spraying – A materials perspective. Acta Materialia. 2016;116:382-407.
[14] Grigoriev S, Okunkova A, Sova A, Bertrand P, Smurov I. Cold spraying: From process fundamentals towards advanced applications. Surface and Coatings Technology. 2015;268:77-84.
[15] Ghelichi R, Bagherifard S, Mac Donald D, Brochu M, Jahed H, Jodoin B, et al. Fatigue strength of Al alloy cold sprayed with nanocrystalline powders. International Journal of Fatigue. 2014;65:51-7.
[16] Ajdelsztajn L, Lavernia E, Jodoin B, Richer P, Sansoucy E. Cold gas dynamic spraying of iron-base amorphous alloy. Journal of thermal spray technology. 2006;15:495-500.
[17] Shayegan G, Mahmoudi H, Ghelichi R, Villafuerte J, Wang J, Guagliano M, et al. Residual stress induced by cold spray coating of magnesium AZ31B extrusion. Materials & Design. 2014;60:72-84.
[18] Li C-J, Li W-Y. Deposition characteristics of titanium coating in cold spraying. Surface and Coatings Technology. 2003;167:278-83.
[19] Eason PD, Kennett SC, Eden TJ, Krull I, Kowalski B, Jones JL. In situ observation of microstrain relief in cold-sprayed bulk copper during thermal annealing. Scripta Materialia. 2012;67:791-4.
[20] Sova A, Grigoriev S, Okunkova A, Smurov I. Potential of cold gas dynamic spray as additive manufacturing technology. The International Journal of Advanced Manufacturing Technology. 2013;69:2269-78.
[21] Stamp R, Fox P, O'neill W, Jones E, Sutcliffe C. The development of a scanning strategy for the manufacture of porous biomaterials by selective laser melting. Journal of Materials Science: Materials in Medicine. 2009;20:1839-48.
[22] Ramirez D, Murr L, Li S, Tian Y, Martinez E, Martinez J, et al. Open-cellular copper structures fabricated by additive manufacturing using electron beam melting. Materials Science and Engineering: A. 2011;528:5379-86.
[23] Blose R, Walker B, Walker R, Froes S. New opportunities to use cold spray process for applying additive features to titanium alloys. Metal Powder Report. 2006;61:30-7.
[24] Morgan RH, Sutcliffe CJ, Pattison J, Murphy M, Gallagher C, Papworth A, et al. Cold Gas Dynamic Manufacturing – A new approach to Near-Net Shape Metal Component Fabrication. MRS Proceedings. 2002;758.
[25] Cadney S, Brochu M, Richer P, Jodoin B. Cold gas dynamic spraying as a method for freeforming and joining materials. Surface and Coatings Technology. 2008;202:2801-6.
[26] MacDonald D, Fernández R, Delloro F, Jodoin B. Cold Spraying of Armstrong Process Titanium Powder for Additive Manufacturing. Journal of Thermal Spray Technology. 2016:1-12.
[27] Lynch ME, Gu W, El-Wardany T, Hsu A, Viens D, Nardi A, et al. Design and topology/shape structural optimisation for additively manufactured cold sprayed components: This paper presents an additive manufactured cold spray component which is shape optimised to achieve 60% reduction in stress and 20% reduction in weight. Virtual and Physical Prototyping. 2013;8:213-31.
[28] Pattison J, Celotto S, Morgan R, Bray M, O'Neill W. Cold gas dynamic manufacturing: A non-thermal approach to freeform fabrication. International Journal of Machine Tools and Manufacture. 2007;47:627-34.

[29] Cormier Y, Dupuis P, Jodoin B, Corbeil A. Net shape fins for compact heat exchanger produced by cold spray. Journal of thermal spray technology. 2013;22:1210-21.
[30] Karthikeyan J, Kay C. Cold spray technology: an industrial perspective. ITSC 2003: International Thermal Spray Conference 2003: Advancing the Science and Applying the Technology2003. p. 117-21.
[31] Marrocco T, McCartney D, Shipway P, Sturgeon A. Comparison of the microstructure of cold sprayed and thermally sprayed IN718 coatings. May; 2006. p. 15-8.
[32] Levasseur D, Yue S, Brochu M. Pressureless sintering of cold sprayed Inconel 718 deposit. Materials Science and Engineering: A. 2012;556:343-50.
[33] Wong W, Irissou E, Vo P, Sone M, Bernier F, Legoux J-G, et al. Cold spray forming of Inconel 718. Journal of thermal spray technology. 2013;22:413-21.
[34] Huang R, Fukanum H. Study of the properties of Cold-Sprayed In718 Deposits. International Thermal Spray Conference 2016. Shanghai- China2016. p. 299-304.
[35] Spierings A, Schneider M, Eggenberger R. Comparison of density measurement techniques for additive manufactured metallic parts. Rapid Prototyping Journal. 2011;17:380-6.
[36] Poza P, Múnez C, Garrido-Maneiro M, Vezzù S, Rech S, Trentin A. Mechanical properties of Inconel 625 cold-sprayed coatings after laser remelting. Depth sensing indentation analysis. Surface and Coatings Technology. 2014;243:51-7.
[37] Hall AC, Cook DJ, Neiser RA, Roemer TJ, Hirschfeld DA. The effect of a simple annealing heat treatment on the mechanical properties of cold-sprayed aluminum. Journal of Thermal Spray Technology. 2006;15:233-8.
[38] Total Materia The world's most comprehensive materials database: Key to Metals AG 2016.

Figure Captions:

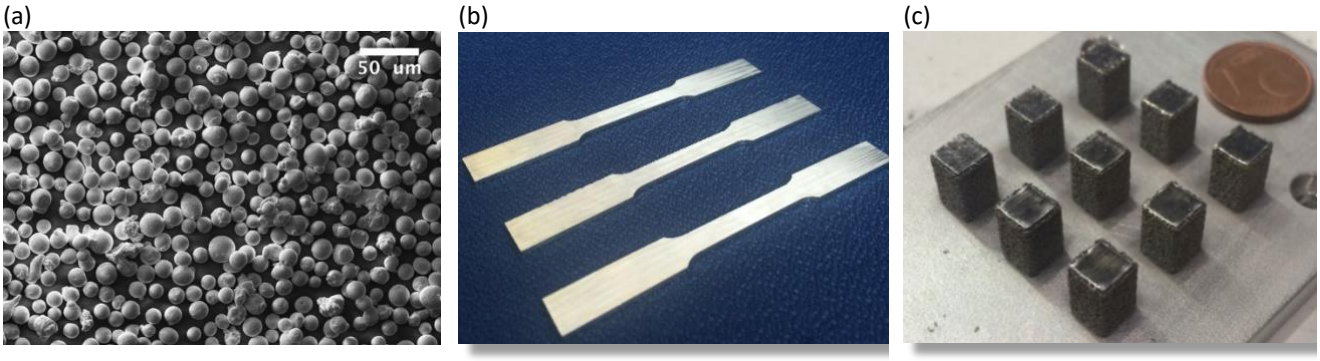

Figure 1. (a) SEM micrograph of Inconel 718 powder used for fabrication of both CS and SLM samples (b) representative dog bone samples obtained from CS deposition (c) cubic samples fabricated by SLM to optimize the process parameters.

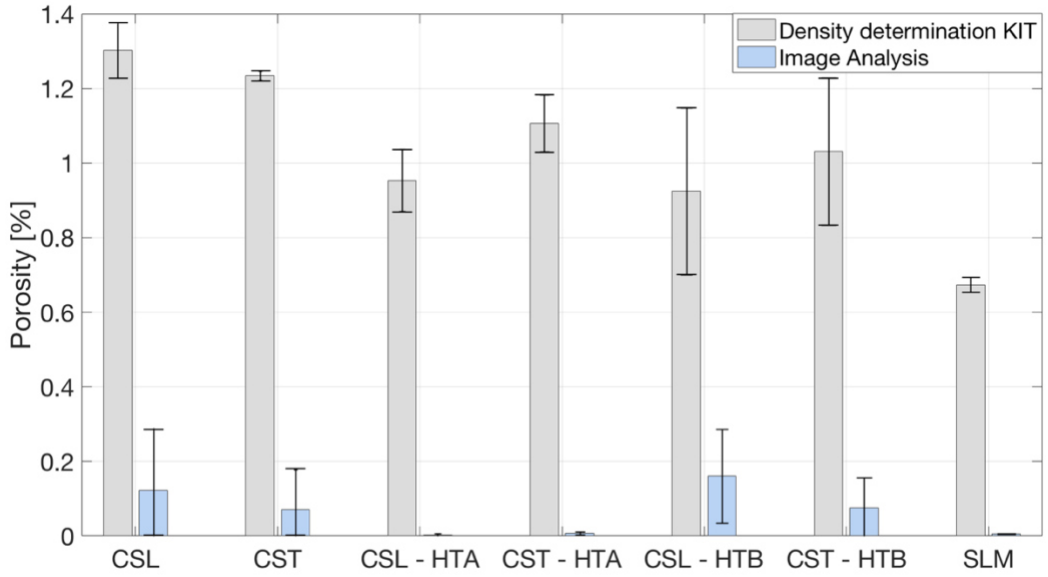

Figure 2. Porosity measurements in all samples using image analysis and density determination kit (optimized SLM condition with 200 W and scan speed of 100 mm/s is depicted).

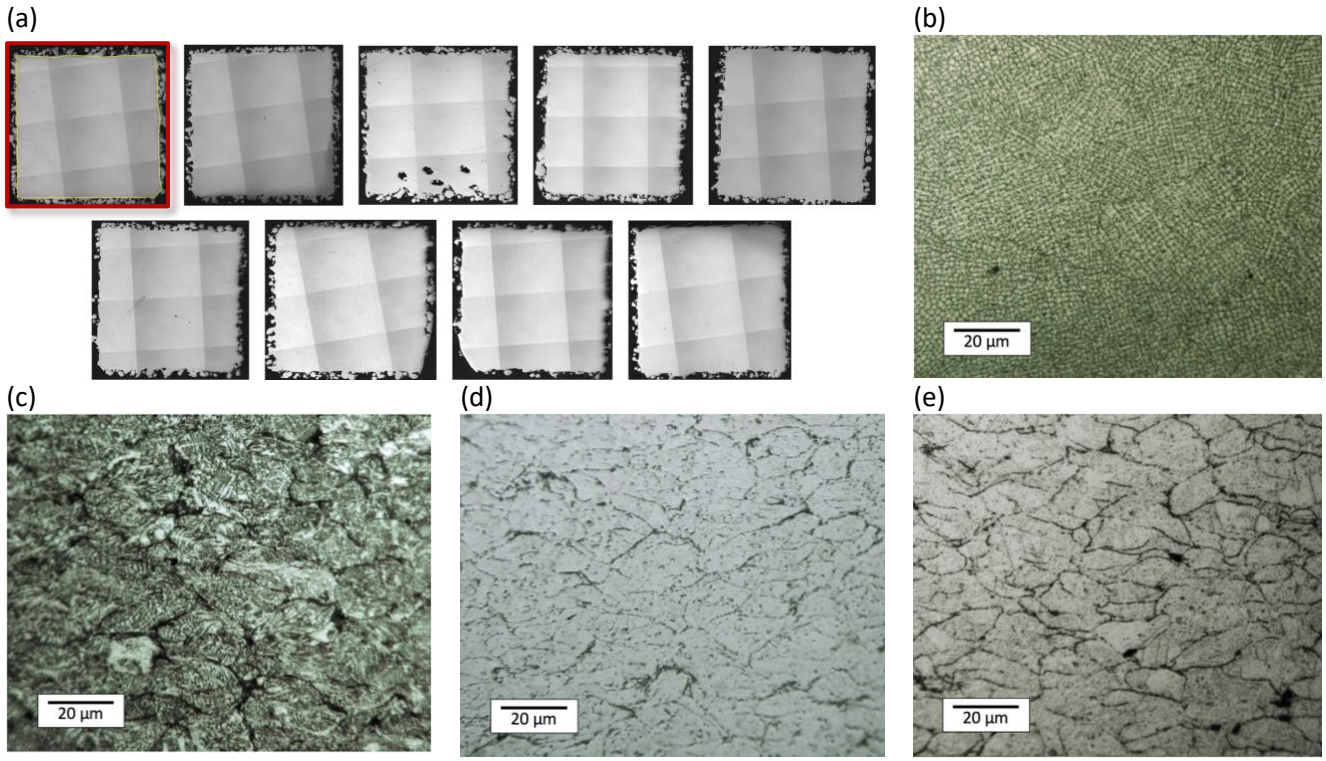

Figure 3. (a) Optical micrographs of SLM cubic samples used for porosity measurements (the yellow line around the sample on the top left indicates an area of 5x5 mm^2 over which porosity measurements have been performed); Cross section optical micrographs representing the microstructure of (b) optimized SLM sample (c) CS longitudinal sample (d) CS longitudinal sample after HTA (e) CS longitudinal sample after HTB.

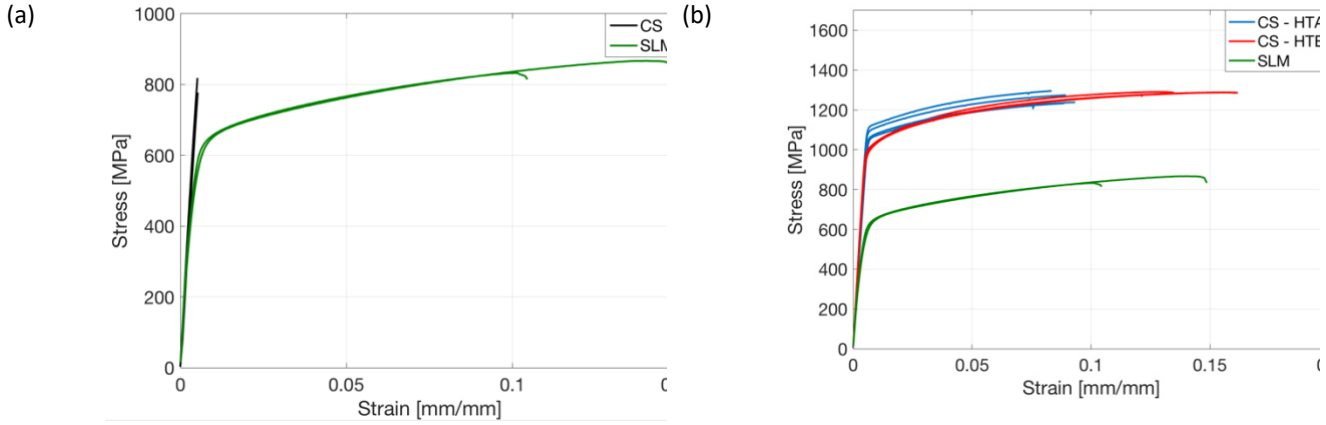

Figure 4. Tensile test data (a) comparison of SLM and CS-before HT samples (b) Comparison of CS sample before and after heat treatments.

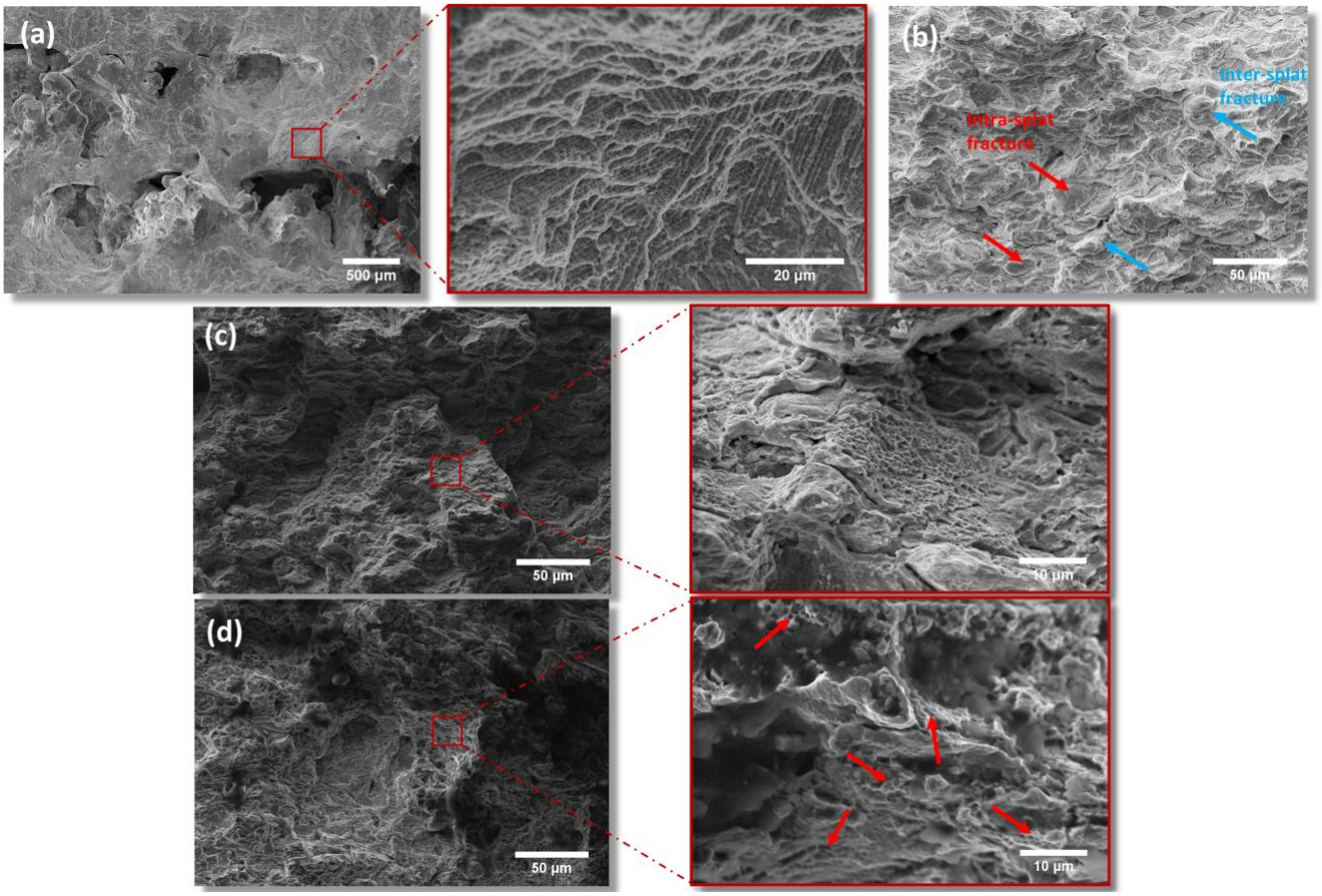

Figure 5. Fractography observation of SLM and CS samples (a)SLM before HT (b) CS before HT (c) CS-HTA (d) CS-HTB

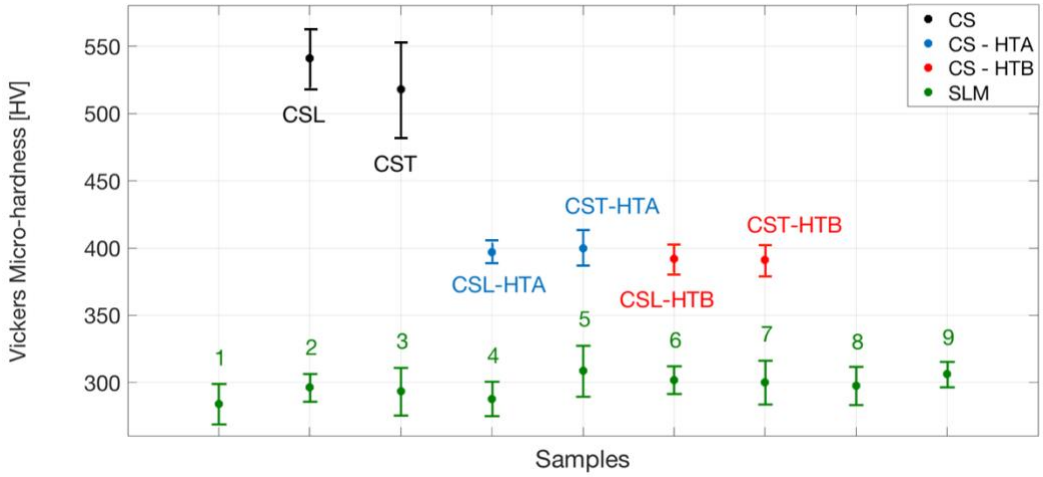

Figure 6. Microharndess measurements performed on SLM cubes and CS samples before and after heat treatments (SLM samples 1: 200 W-100 mm/s; 2: 200 W-150 mm/s; 3: 200 W-200 mm/s; 4: 250 W-100 mm/s; 5: 250 W-150 mm/s; 6: 250 W-200 mm/s; 7: 300 W-100 mm/s; 8: 300 W-150 mm/s; 9: 300 W-200 mm/s).

(a) (b)

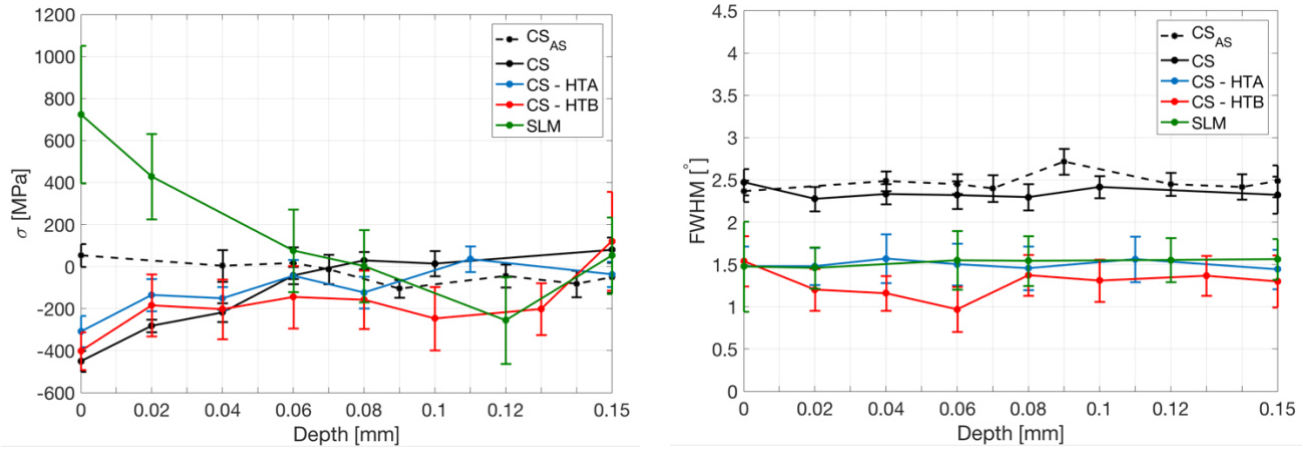

Figure 7. In-depth distribution of (a) residual stresses (b) FWHM in the SLM and CS samples (CS_{AS} is the as sprayed cold sprayed sample before machining)

Tables:

Table 1. List of process parameters for preparation of CS deposits

Cold spray parameters	
Gas temperature (ºC)	1000
Gas	N_2
Gas pressure (bar)	55
Traverse velocity (mm/s)	500
Track spacing (mm)	1
Standoff distance (mm)	25

Table 2. Main specifications of the prototype SLM system.

Laser emission wavelength	1070 nm
Max. laser power	1000 W
Beam quality factor, M^2	5.14
Delivery fiber diameter	50 µm
Collimation lens	60 mm
Focal lens	255 mm
Nominal beam diameter on focal plane	212 µm
Build platform area (DxWxH)	60x60x20 mm^3

Table 3. List of selective laser melting parameters for preparation of SLM deposits.

Selective laser melting parameters	
Focal position (mm)	0
Layer thickness (µm)	50
Hatch distance (µm)	110
Laser power (W)	200; 250; 300
Scan speed (mm/s)	100; 150; 200

Table 4. Tensile test data for SLM and CS samples before and after heat treatments compared to reference bulk material

	CS before HT		CS HTA		CS HTB		SLM	Bulk material [38]
	L	T	L	T	L	T		
Ultimate tensile strength (MPa)	797±20	627±100	1264±30	1256±18	1298±2	1288±0	850±15	≥1240
Yield strength (MPa)	-	-	1091±30	1083±15	1004±5	1004±7	580±10	≥1000
Young's modulus (GPa)	167±9	167±0.1	190±11	193±5.5	203±12	201±0.8	165±8.8	211
Strain at break (%)	0.5	0.4±0.1	8.6±0.3	9.1±0.2	14.5±0.95	16.2±0.05	12.6±2.2	≥12